Exciton Dynamics in Semiconducting Carbon Nanotubes

ARTICLE *in* THE JOURNAL OF PHYSICAL CHEMISTRY B · NOVEMBER 2010

Impact Factor: 3.3 · DOI: 10.1021/jp106250a · Source: PubMed

8 AUTHORS, INCLUDING:

Alexander Green
Harvard University
66 PUBLICATIONS **3,888** CITATIONS

SEE PROFILE

THE JOURNAL OF PHYSICAL CHEMISTRY B

ARTICLE

pubs.acs.org/JPCB

Exciton Dynamics in Semiconducting Carbon Nanotubes

M. W. Graham,[‡] J. Chmeliov,[§] Y.-Z. Ma,[‡,∥] H. Shinohara,[⊥] A. A. Green,[#] M. C. Hersam,[#] L. Valkunas,*[,§] and G. R. Fleming[‡]

[‡]Department of Chemistry, University of California, Berkeley, and Physical Biosciences Division, Lawrence Berkeley National Laboratory, Berkeley, California 94720-1460, United States

[§]Center for Physical Sciences and Technology, Savanoriu Ave. 231, 02300 Vilnius, Lithuania, and Theoretical Physics Department, Faculty of Physics of Vilnius University, Sauletekio Ave. 9, build. 3, 10222 Vilnius, Lithuania

[∥]Chemical Sciences Division, Oak Ridge National Laboratory, Oak Ridge, Tennessee 37831-6201, United States

[⊥]Department of Chemistry and Institute for Advanced Research, Nagoya University, Furo-Cho, Chikusa-ku, Nagoya 464-8602, Japan

[#]Department of Materials Science and Engineering, Northwestern University, Evanston, Illinois 60208, United States

ABSTRACT: We report a femtosecond transient absorption spectroscopic study on the (6, 5) single-walled carbon nanotubes and the (7, 5) inner tubes of a dominant double-walled carbon nanotube species. We found that the dynamics of exciton relaxation probed at the first transition-allowed state (E_{11}) of a given tube type exhibits a markedly slower decay when the second transition-allowed state (E_{22}) is excited than that measured by exciting its first transition-allowed state (E_{11}). A linear intensity dependence of the maximal amplitude of the transient absorption signal is found for the E_{22} excitation, whereas the corresponding amplitude scales linearly with the square root of the E_{11} excitation intensity. Theoretical modeling of these experimental findings was performed by developing a continuum model and a stochastic model with explicit consideration of the annihilation of coherent excitons. Our detailed numerical simulations show that both models can reproduce reasonably well the initial portion of decay kinetics measured upon the E_{22} and E_{11} excitation of the chosen tube species, but the stochastic model gives qualitatively better agreement with the intensity dependence observed experimentally than those obtained with the continuum model.

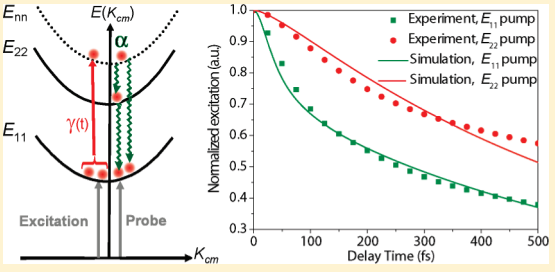

I. INTRODUCTION

Depending on the strength of the Coulombic interaction, the elementary excitation in solid states can be either a neutral exciton or a pair of electrons (e) and holes (h) with a weak mutual correlation.[1] A quantitative measure of the Coulombic interaction is the exciton binding energy (E_b), defined as the energy difference between the e−h continuum and the lowest bound exciton state. As deduced experimentally[2,3] and from *ab initio* calculations,[4,5] the E_b value determined for semiconducting single-walled carbon nanotubes (SWNTs) typically ranges from 0.3 to 1 eV, permitting assignment of the dominant absorption/emission spectral bands to excitonic transitions. Such large E_b values are possible because of greatly enhanced electron−hole Coulombic interactions owing to quasi-one-dimensional (quasi-1-D) confinement in SWNTs.[6]

Experimental studies of the excitation dynamics in the SWNT employing ultrafast transient absorption[7−10] and time-resolved fluorescence techniques with sub-100-fs time resolution[11,12] reveal a very fast kinetic decay component on the time scale of a few hundreds of femtoseconds. Through analysis of both the nonexponential kinetic decay component and the dependence of the corresponding amplitude on excitation intensity, it was concluded that exciton−exciton annihilation in semiconducting SWNTs is a dominant relaxation process.[10,11,13,14]

The exciton energy, $E^n_{cv}(K_{CM})$, in semiconducting SWNTs is typically characterized by the translation wavenumber K_{CM}, which satisfies the translation symmetry of the center of mass of the e−h pair, and the quantum number n corresponding to their relative motion (1s, 2p, ... states of the hydrogen type spectrum).[1] The subscripts c and v refer to the corresponding van Hove singularities in the conduction and valence bands, respectively.[4,5] These exciton states are the eigenstates of electronic excitation, which are delocalized over the system under consideration. Thus, any exciton evolution should be determined by their interactions with phonons, impurities, or scattering with other excitons resulting in exciton−exciton annihilation. This nonlinear annihilation process involves a pair of excitons whose interaction leads to rapid relaxation of one exciton, whereas the other is promoted to a doubly excited state $E_{nn} \cong 2E_{11}$ owing to momentum and energy conservation (see Figure 1a). A theoretical description of an exciton−exciton annihilation process would then define the transitions between the bands of the multiexciton manifolds resonantly coupled with other excited states, which decay by subsequent linear relaxation due to electron−phonon coupling.[13]

The evolution of the occupation probability of these multiexciton states and the annihilation rate constant are the main

Special Issue: Shaul Mukamel Festschrift

Received: July 6, 2010
Revised: September 13, 2010
Published: November 23, 2010

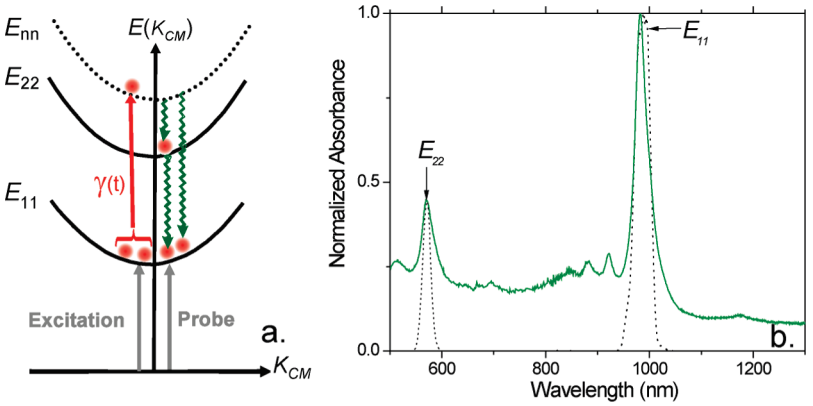

Figure 1. (a) Schematic energy level diagram of a semiconducting SWNT with a dominant relaxation pathway mediated by exciton−exciton annihilation (with a rate constant $\gamma(t)$), shown for the direct E_{11} excitation case. (b) Linear absorption spectrum of the (6, 5) tube-enriched aqueous solution and laser pulse spectra (dotted line) resonant with either its E_{22} or E_{11} transition.

characteristics of a stochastic model. According to this description, exciton−exciton annihilation manifests itself as long as more than one exciton is present in the system but switches off when a single exciton is finally left.[15,16] Such a scheme is well suited for describing the exciton decay kinetics at times shorter than 10 ps.[10,11,14] On the other hand, it has also been demonstrated that the exciton decay kinetics on a longer time scale (up to 1 ns) follows diffusion-controlled behavior.[17,18] In addition, calculations based on a diffusion-controlled exciton−exciton annihilation model enabled reproduction of the saturation behavior of photoluminescence emission with increasing excitation intensity.[19,20] Moreover, a recent study of the intensity-dependent exciton decay further suggested that exciton−exciton annihilation in semiconducting SWNTs is an inefficient process.[21] Apparently, these conclusions differ greatly from the conclusions derived from the earlier studies,[7−12] and are also inconsistent with the conclusions drawn from recent four-wave-mixing spectroscopic experiments at different excitation intensities.[22,23] In order to provide clarity to these conflicting studies, we carried out analyses of the exciton decay kinetics on different time scales and at different excitation intensities.

II. MATERIALS AND METHODS

The SWNT sample used in this study is highly enriched in a single semiconducting tube type, the (6, 5) nanotube, which was isolated through density-gradient ultracentrifugation.[24] The obtained aqueous solution contains individually separated nanotubes, which were dispersed with sodium cholate as a surfactant. The experiments were performed either directly using the aqueous suspensions with a 200 μm path length cell or on a thin composite film fabricated by mixing the aqueous solution with an appropriate amount of water-soluble polyvinylpyrrolidone (PVP) polymer. Use of the polymer film samples enabled us to carry out measurements at low temperatures with a Janis cryostat, which was operated under continuous liquid helium flow. Measurements of linear absorption and steady-state fluorescence emission spectra confirm that the nanotubes remain individualized after being transferred from the solution to the solid film, and the SWNT/PVP composite films retain an optical quality at cryogenic temperatures as low as 4.4 K. The double-walled carbon nanotubes (DWNTs) were prepared by chemical vapor deposition in combination with thermal oxidation to greatly reduce the presence of SWNTs.[25] The purified DWNTs were dispersed individually in D_2O solution using sodium dodecyl sulfate (SDS) as a surfactant, and have ~90% DWNT content. A quartz sample cell of 1 mm path length was used for measurements on the DWNT samples. Here, we examine only the (7, 5) tube, the inner tube of a dominant DWNT species in the sample, through resonant excitation of its corresponding E_{11} and E_{22} transitions. The inclusion of the DWNTs in our study allowed us to not only probe the dynamics of a different tube type but also elucidate the effect of the local environment arising from the presence of an outer tube species.

The femtosecond transient absorption setup employed here has been described extensively elsewhere.[13,26] In short, the light source was an optical parametric amplifier pumped by a 250 kHz Ti:sapphire regenerative amplifier, which enabled resonant excitation of either the E_{11} or E_{22} transitions of selected nanotube species with a 50 fs laser pulse (full width at half-maximum, fwhm). The pump beam was focused to a spot with a diameter of 161 μm at the sample. A single-filament white-light continuum served as the probe beam, and selection of the probe wavelength was realized using a single-grating monochromator with a typical bandwidth of 8 nm. The detection scheme consists of a Si photodiode and a lock-in amplifier. The polarization of the pump beam was set to the magic angle (54.7°) with respect to the probe beam. A combination of a waveplate and polarizer was used to control the intensity of the pump laser beam.

III. EXPERIMENTAL OBSERVATIONS

Figure 1b shows the linear absorption spectrum of the (6, 5) tube-enriched, individualized SWNTs in aqueous solution. The two bands peaking at 982 and 570 nm correspond to the E_{11} and E_{22} excitonic transitions of the (6, 5) tube type, respectively. Upon resonant excitation of these bands with ultrashort laser pulses (see the dotted lines in Figure 1b for the laser pulse spectra), a series of transient absorption kinetics were probed at 988 nm under different pump intensities. As observed previously, the transient absorption signals ($\Delta OD(t)$) are dominated by photobleaching and stimulated emission.[27] Also, consistent with previous work, the kinetic profiles are, after normalizing at the signal maxima (ΔOD_0), largely invariant to the excitation intensity for each chosen pump wavelength.[10] However, the amplitudes of the signal maxima show strikingly different dependence on the pump laser intensity for the E_{11} and E_{22} pump cases, as shown in Figure 2. A linear dependence of the amplitude on the intensity of the E_{22} excitation was found, whereas for the E_{11} excitation the corresponding amplitude scales linearly with the square root of the intensity. In both cases, the amplitudes of signal maxima exhibit saturation behavior when the excitation intensity is greater than $\sim 1.4 \times 10^{13}$ photons/cm^2. The same intensity dependence was also found for the SWNT/PVP

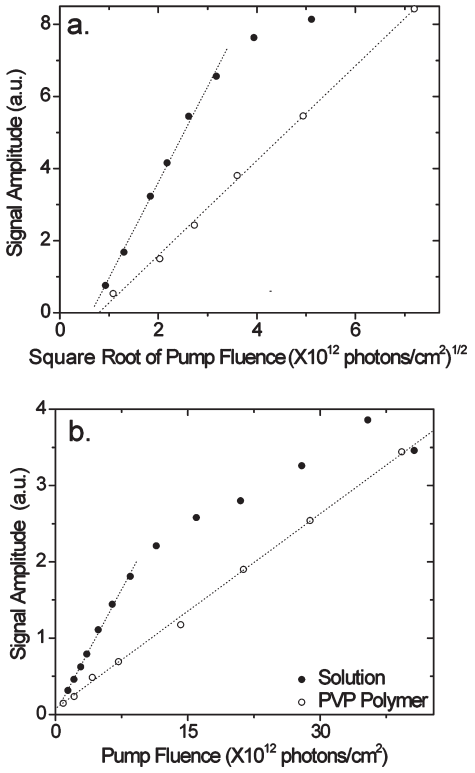

Figure 2. (a) Plots of the maximal transient absorption signals measured at 988 nm as a function of the square root of pump fluence for the (6, 5) tube species upon E_{11} excitation. The samples were either a polymer−SWNT composite film (open circles) or an aqueous solution (filled circles). (b) Plots of the maximal transient absorption signals measured at 988 nm as a function of the pump fluence for the (6, 5) tube species upon E_{22} excitation.

composite film (see the open circles in Figure 2). In this case, the absence of the saturation behavior due to high sample optical density makes the different intensity dependence found for the E_{11} and E_{22} excitation even more distinct.

Quantitative data analysis employing a least-squares deconvolution fitting algorithm with explicit consideration of the finite temporal response shows that all of the decay kinetics can be satisfactorily described with a model function consisting of three or four exponents. The component with the longest lifetime typically has a time scale of a few hundred picoseconds, which characterizes the relaxation associated with the last remaining exciton in the system. The kinetics probed at room temperature for the E_{11} transition of the (6, 5) tube upon excitation of its E_{22} state exhibits a slower initial decay than the corresponding kinetics measured with direct E_{11} excitation (Figure 3a). In particular, the two fast decay components have considerably different decay time scales (and relative amplitude). These are 122 fs (55%) and 1.3 ps (29%) for E_{11} excitation and 350 fs (57%) and 2.4 ps (31%) for E_{22} excitation. In contrast, the two slow decay components appear similar for the two pump wavelengths, with decay times of ∼22 and ∼300 ps, respectively.

The kinetics measured at temperatures down to 4.4 K show a similar trend with the change of pump intensity as observed at 292 K (in Figure 2) for both the E_{22} and E_{11} pump cases (data not shown). A representative set of transient absorption profiles measured at 110 K is plotted in Figure 3b, where a remarkably faster decay is seen for the E_{11} pump case than the one obtained with the E_{22} pump. The lifetimes (relative amplitudes) determined from deconvolution fitting are 140 fs (63%), 1.5 ps (29%), and 19 ps (8%) for the E_{11} excitation data, whereas the corresponding results are 310 fs (52%), 2.1 ps (28%), and 22.4 ps (20%) for E_{22} excitation.

The need for multiple (three or four) exponential components to satisfactorily fit the transient absorption kinetics is due, in part, to the occurrence of nonlinear exciton−exciton annihilation.[13] A qualitative justification can be obtained by assuming that the exciton−exciton annihilation process dominates the kinetic decay, and in this case a simple rate equation for exciton density $n(t)$ can be written as $dn(t)/dt = -(1/2)\gamma t^{d/2-1} n^2(t)$, where γ is the time-independent annihilation rate and d is the dimensionality.[11] As the transient absorption signal ($\Delta OD(t)$) at a given delay time t is proportional to $n(t)$, for a 1-D system ($d = 1$) the solution of the rate equation suggests a linear relation when the transient absorption signal is plotted in the form of $(\Delta OD_0/\Delta OD(t) - 1)^2$ versus delay time t (ΔOD_0 is the signal amplitude at $t = 0$). As shown in Figure 3c, a good linear relation is indeed seen for the data collected with E_{11} excitation when t is approximately greater than 1 ps (green circles). This linear behavior suggests diffusion-limited annihilation in a 1-D system. In comparison, the data obtained with the E_{22} pump exhibit a relatively large deviation from linearity (filled black circles), suggesting a substantial contribution from linear relaxation to the ground state. Upon cooling, the data collected with the E_{22} pump at 110 K again show good linear relation in the plot of $(\Delta OD_0/\Delta OD(t) - 1)^2$ versus delay time within the experimental uncertainty (see Figure 3d, black circles). In strong contrast, the result obtained with the E_{11} pump at the same temperature exhibits an excellent linear relation between $(\Delta OD_0/\Delta OD(t) - 1)$ and delay time t (Figure 3d, green circles). The latter linear relation can be derived from the same rate equation but for $d = 2$ and a resultant time-independent annihilation rate constant. As discussed in our earlier work, this time-independent annihilation rate arises from a rapid annihilation process involving coherently delocalized excitons.[13,28]

The difference between the kinetics probed at the E_{11} state upon excitation of the E_{11} and E_{22} states at room temperature is much more pronounced for the (7, 5) inner tube of the DWNT species (see Figure 4a for the DWNT data). Here, the dominant and fastest decay component has a lifetime of 110 fs for the E_{11} pump, whereas it is 800 fs for the E_{22} pump. It is also noteworthy that the kinetics probed for the (7, 5) inner tube exhibits a substantially slower decay than the decay of the (7, 5) SWNT type measured under a similar excitation intensity (see the black trace in Figure 4a, for example). Our measurements under different excitation intensities for the (7, 5) inner tube of the DWNT species show a linear dependence of the maximum transient absorption amplitude on the intensity of the E_{22} excitation (Figure 4b, open circles) and a square root dependence on the intensity of E_{11} excitation (Figure 4b, filled circles). These observations parallel those found in SWNTs such as the (6, 5) tube type, as shown in Figure 2, suggesting the distinct intensity dependence may be a generic phenomenon for semiconducting nanotubes. Moreover, a plot of the kinetics measured for the (7, 5) inner tube with E_{11} excitation (black line in Figure 4a) in the form of $(\Delta OD_0/\Delta OD(t) - 1)^2$ vs delay time t gives a good linear relationship for the first few picoseconds (see Figure 4c, inset). As with the (6, 5) tube type (see Figure 3c,d), this linear relation again suggests the occurrence of diffusion-limited annihilation. However, at short times, deviation from linearity is again noticeable. This can be more clearly seen from a plot of the same data as a function of the inverse of the square root of delay time, $1/\sqrt{t}$ (see Figure 4c). The initial decay within the first 600 fs does not follow the linear dependence (indicative of diffusion-controlled annihilation) seen at longer delay times.

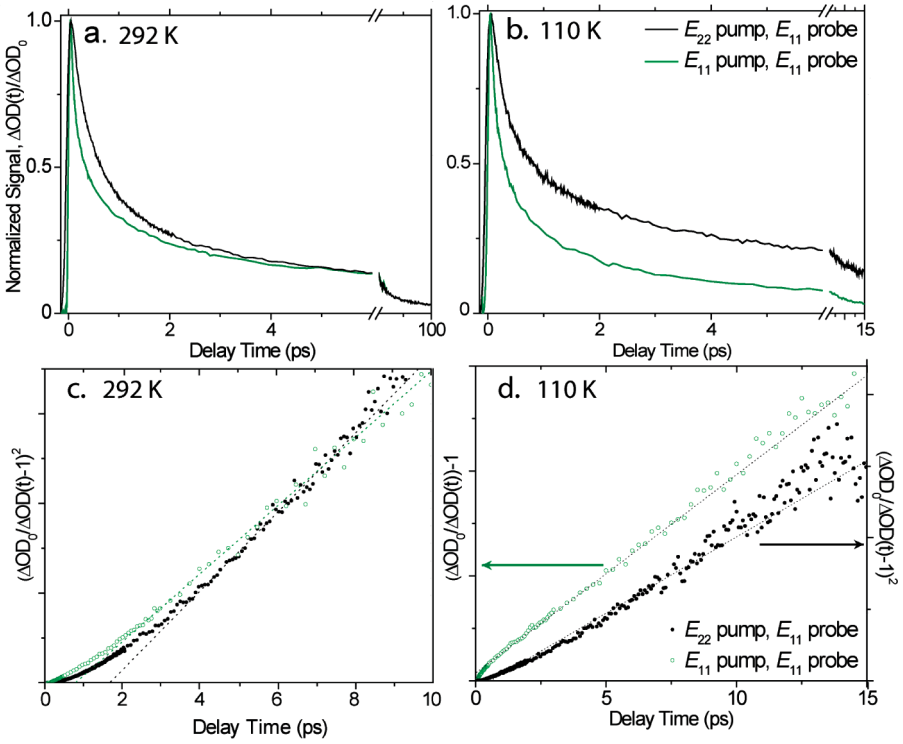

Figure 3. Transient absorption kinetics measured upon resonant excitation of the E_{11} state at 988 nm and the E_{22} state at 570 nm, respectively, for the (6,5) tube species. (a) Data acquired at 292 K for an aqueous solution sample and (b) at 110 K for a PVP polymer composite film. (c) Plotting the same data shown in (a) as $(\Delta OD_0/\Delta OD(t) - 1)^2$ versus delay time. The dashed lines are linear fits to the majority of data points. (d) Plotting the same data shown in (b) as $(\Delta OD_0/\Delta OD(t) - 1)$ (left axis) or $(\Delta OD_0/\Delta OD(t) - 1)^2$ (right axis) versus delay time.

IV. THEORETICAL DESCRIPTION OF EXCITON−EXCITON ANNIHILATION

The key findings of our transient absorption measurements on the (6, 5) SWNT species and the (7, 5) inner tube of a dominant DWNT type are as follows. First, we found that the initial decay of the kinetics probed at the E_{11} state of the (6, 5) tube species upon excitation of its corresponding E_{22} transition is clearly slower than that measured with its direct E_{11} excitation (see Figure 3a,b), and this difference appears much more pronounced for the (7, 5) inner tube type (Figure 4a). Second, the maximal signal amplitudes scale linearly with the intensity of the E_{22} excitation but with the square root of the E_{11} excitation intensity (see Figures 2 and 4b). Our qualitative analysis further shows the occurrence of a diffusion-limited annihilation process except for the data collected at 110 K for direct E_{11} excitation (Figure 3d, green circles). In order to gain insight into this strikingly different temporal and intensity behavior in response to the different excitonic states initially excited, we now develop a detailed theoretical description with explicit consideration of exciton−exciton annihilation.

Continuum Model. Exciton−exciton annihilation is typically described in terms of a simple scheme, which is well justified for extended systems.[10,13,29] The time evolution of excitons in this approach can be determined by the following kinetic equations:

$$\begin{aligned} \frac{dn_1}{dt} &= G_1(t)f_1(n_1) - Kn_1 - \gamma(t)n_1^2 + k_{21}f_1(n_1)n_2 \\ \frac{dn_2}{dt} &= G_2(t)f_2(n_2) + k_{n2}f_2(n_2)n_n - k_{21}f_1(n_1)n_2 \\ \frac{dn_n}{dt} &= \frac{1}{2}\gamma(t)n_1^2 - k_{n2}n_nf_2(n_2) \end{aligned} \quad (1)$$

where n_i is the exciton concentration populating the ith exciton state (the E_{ii} state), $G_i(t)$ is the generating function of the pump pulse (depending on the resonance condition corresponding to the E_{ii} state), $f_i(n_i) = 1 - (n_i/N_i)$ is the phase space-filling factor (N_i determines the maximal amount of excitations, which can be generated in the ith state), $\gamma(t)$ is the rate of exciton−exciton annihilation (on the E_{11} exciton state), and the linear relaxation terms determine the dominant relaxation pathways. K is the relaxation rate for the E_{11} exciton, and k_{21} determines the rate of the relaxation from the E_{22} state to the E_{11} state. Here, the E_{nn} state corresponds to the excited state, which is involved in the process of exciton−exciton annihilation ($E_{nn} \cong 2E_{11}$ shown in Figure 1a), and k_{n2} determines the rate of the exciton transfer between the corresponding states. In the case of short pump pulses (when the pump pulse duration is shorter than $1/k_{21}$ and $1/k_{n2}$), the excitation intensity dependence of the initial populations will be different for different pump conditions. If the pump pulse is in resonance with the E_{11} exciton state, then $G_2(t) = 0$, and if also the time dependence of the annihilation rate can be discarded, at high excitation conditions (when the nonlinear exciton relaxation due to exciton−exciton annihilation is dominating) but not so high that the phase filling starts to manifest itself, i.e., when $n_1 \ll N_1$ is still fulfilled and, thus, $f_1(n_1) \approx 1$, from eq 1 it follows that

$$n_1(0) \approx \sqrt{\frac{G_{1,\max}}{\gamma}} \quad (2)$$

where $G_{1,\max}$ is the maximal value of the generating function. Due to the short pulse duration (in comparison with $1/k_{21}$ and $1/k_{n2}$), the E_{22} state is not populated at the initial times, i.e., $n_2(0) \approx 0$. In the opposite case, when the pump pulse is in resonance with the E_{22}

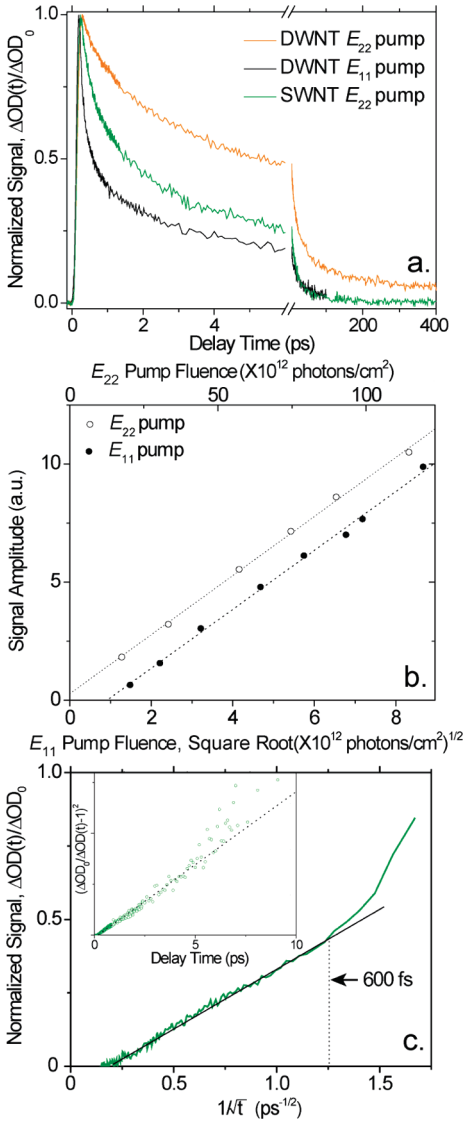

Figure 4. (a) Comparison of transient absorption kinetics obtained for the (7, 5) inner tube of a dominant DWNT species upon E_{22} (orange) and E_{11} (black) excitation with the one measured for the (7, 5) SWNT (dark green) following excitation of its E_{22} state. (b) Plot of the peak amplitudes obtained upon the E_{11} (filled circles) or E_{22} (open circles) excitation for the (7, 5) inner tube of the dominant DWNT species as a function of the square root of pump fluence or pump fluence, respectively. (c) The data measured for the (7, 5) inner tube upon E_{11} excitation is plotted as a function of the inverse of the square root of delay time. The inset shows the same data plotted as $(\Delta OD_0/\Delta OD(t) - 1)^2$ versus delay time.

exciton state, we have $G_1(t) = 0$, and then

$$n_2(0) \approx \frac{G_{2,\max}}{k_{21}} \tag{3}$$

while $n_1(0) \approx 0$. Here, $G_{2,\max}$ is the maximal value of the generating function.

The transient spectrum $\Delta OD(t,\lambda)$ is defined by the exciton populations and, thus, can be given by[13,29]

$$\Delta OD(t,\lambda) \propto \sum_i n_i(t)[\sigma_i^{ESA}(\lambda) - \sigma_i^{SE}(\lambda) - \sigma_0(\lambda)] \tag{4}$$

where $\sigma_0(\lambda)$ is the ground state absorption spectrum (λ is the wavelength of the probe pulse), $\sigma_i^{ESA}(\lambda)$ and $\sigma_i^{SE}(\lambda)$ are the cross sections for excited state absorption and stimulated emission of the ith excited state, respectively, $n_i(t)$ determines the time evolution of the ith excited state population according to eq 1 (i enumerates the exciton states populated by excitation pulses, relaxation from higher states and via exciton−exciton annihilation). Thus, by substituting eq 2 into eq 4, we will get that the transient bleaching amplitude should be proportional to $(G_{1,\max})^{1/2}$, while by substituting eq 3 into eq 4 we will get the result proportional to $G_{2,\max}$. This qualitatively is in line with the experimental dependences shown in Figure 2.

Due to the finite rate k_{21} of the exciton relaxation from the E_{22} exciton state to the E_{11} state (in comparison with the pump pulse duration), the situation corresponding to the E_{22} excitation can be considered in a similar way as in the case of direct E_{11} excitation but with longer pulses. This should evidently slow down the decay kinetics in accord with the experimental observations shown in Figure 3.

The ground state bleaching should be proportional to $(n_1 + n_2)_{\max}$, where the subscript indicates the maximal value, as follows from eq 4. For modeling, we use a Gaussian pump pulse with amplitude A and fwhm duration of 50 fs. Taking typical values such as $k_{21}^{-1} \approx 50$ fs,[30] $\gamma^{-1} = 800$ fs for two excitons per nanotube,[12] $K^{-1} \approx 10$ ps, and assuming that $k_{n2} \gg k_{21}$, we cannot obtain the intensity dependence as shown in Figure 2 for the pulse durations of the order of tens of fs. At high excitation intensities, we generally found that $n_{2\max} > n_{1\max}$ independent of either E_{11} or E_{22} state being initially excited. Furthermore, in both cases, the calculated amplitude of the bleaching signal always follows almost linear intensity dependence, and change of the parameters used in our calculations does not alter this result. This clear discrepancy from the experimental data can be improved by modifying the annihilation kinetic scheme described by eq 1 through assuming existence of two pathways of the exciton relaxation from the $E_{nn} \cong 2E_{11}$ state: one via population of the E_{22} exciton state and another directly to the E_{11} exciton state bypassing the E_{22} exciton state. Such a branching scheme for the exciton relaxation from the $E_{nn} \cong 2E_{11}$ state in combination with an assumption of similarly high relaxation rates can be described by slightly modifying the kinetic equations given by eq 1:

$$\begin{aligned} \frac{dn_1}{dt} &= G_1(t)f_1(n_1) - Kn_1 - \frac{1}{2}(1+\alpha)\gamma(t)n_1^2 + k_{21}f_1(n_1)n_2 \\ \frac{dn_2}{dt} &= G_2(t)f_2(n_2) + \frac{1}{2}\alpha\gamma(t)n_1^2 - k_{21}f_1(n_1)n_2 \end{aligned} \tag{5}$$

where α determines the branching ratio. The intensity dependence of the $(n_1 + n_2)_{\max}$ value obtained resembles the experimental observations for both excitation conditions (Figure 5a) when the phase-filling effects are neglected and assuming relatively small α values, e.g., $\alpha = 0.1$. However, the same set of parameters produces a much faster decay behavior than the kinetics observed experimentally, as shown in Figure 3. Better agreement at least for the initial delay times can be obtained by assuming that the relaxation rate, k_{21}, is up to 10 times slower. The best fit of the experimental kinetics measured at 292 K is obtained for the following parameters, which are treated as variables: $\alpha = 0.4$, $\gamma^{-1} = 1040$ fs, $k_{21}^{-1} = 480$ fs (Figure 5b). An excitation intensity of $G_{\max} \equiv A = 8$ is used for our calculations. Similarly, for the kinetics measured at 110 K, we obtain $\alpha = 0.5$, $\gamma^{-1} = 3760$ fs, and $k_{21}^{-1} = 410$ fs for the same excitation intensity (Figure 5c). We further found that an increase of the A value from 1 to 30 leads to almost linear variation of the corresponding $1/\gamma$ value with A. The intensity dependences of

dx.doi.org/10.1021/jp106250a |J. Phys. Chem. B 2011, 115, 5201–5211

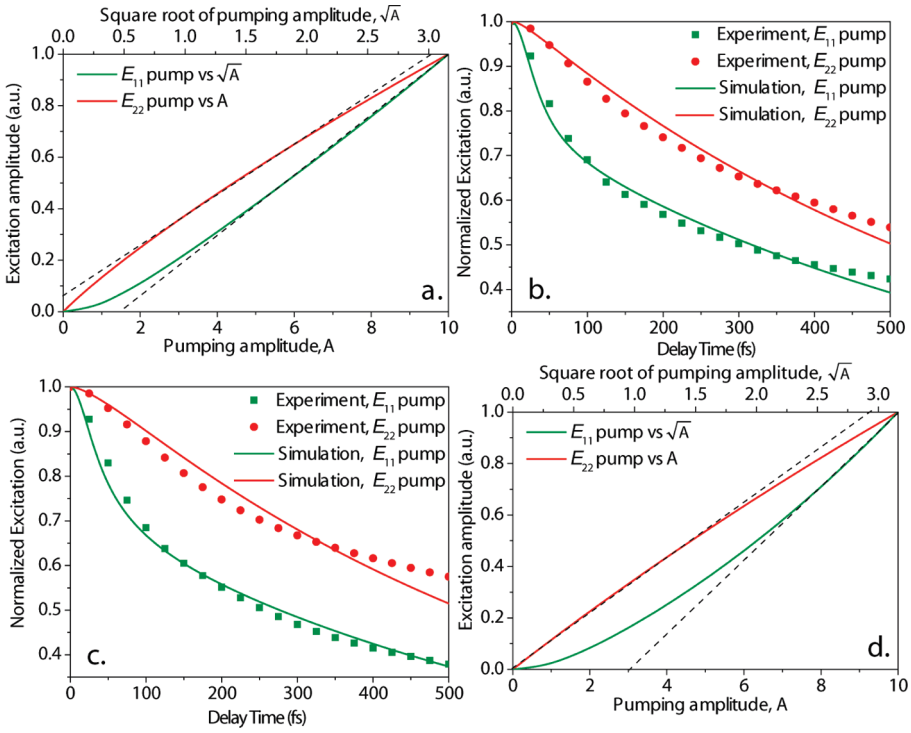

Figure 5. (a) The dependence of $(n_1 + n_2)_{max}$ calculated according to the continuum model (eq 5) with typical values of γ^{-1} = 800 fs, k_{21}^{-1} = 50 fs, and assuming $\alpha = 0.1$ on the pump pulse intensity A in the case of pumping to the E_{22} band (red curve, lower x-axis) and of its square root $\sqrt{A}$ in the case of pumping to the E_{11} band (green curve, upper x-axis). (b) The best fit for both experimental kinetics measured at room temperature (292 K) upon excitation of the E_{11} or E_{22} band (green and red curves, respectively) is obtained using the following parameters: $\alpha = 0.4$, γ^{-1} = 1040 fs, k_{21}^{-1} = 480 fs, and an amplitude of the generation function $A \equiv G_{max} = 8$. (c) The best fit for the corresponding kinetics measured at 110 K is obtained by assuming the same intensity of the generation function, A, and using the following parameters: $\alpha = 0.5$, γ^{-1} = 3760 fs, and k_{21}^{-1} = 410 fs. (d) The dependence of the $(n_1 + n_2)_{max}$ on the pump pulse intensity A in the case of the E_{22} excitation (red curve, lower x-axis) and on its square root $\sqrt{A}$ in the case of the E_{11} excitation (green curve, upper x-axis) calculated using the same set of parameters. This dependence is almost the same for the kinetics measured at different temperatures.

$(n_1 + n_2)_{max}$ calculated using the same sets of parameters are very similar for both cases and qualitatively agree with the experimental observations, as shown in Figure 5d.

The calculated kinetics, however, start to substantially deviate from the experimental kinetics on a longer time scale (>400 fs). The calculated decays are much faster than our experimental data, which suggests an overestimation of the efficiency of exciton−exciton annihilation processes at longer time scales. To avoid such fast excitation decay, a stochastic description of the exciton−exciton annihilation process should be used instead.[13]

Stochastic Model. This model describes the population probabilities[13] according to the scheme shown in Figure 6. In the case of multiple excitons in the system, they can populate both E_{11} and E_{22} states in the course of their generation/relaxation. To reflect these relaxation/generation pathways, various energy levels $E_{i,j} = i \cdot E_{11} + j \cdot E_{22}$ have to be taken into account, as shown in Figure 6, where i and j specify the amount of excitons in the E_{11} and E_{22} bands, respectively. The possible transition pathways between various energy levels determining the evolution of probabilities, $P_{i,j}$, are depicted by arrows. Time-dependent rates of the exciton generation in the E_{11} and E_{22} bands already containing i and j excitons are defined as $G_1^{(i)}(t)$ and $G_2^{(j)}(t)$, respectively, while the relaxation rate $k_{21}^{(j)}$ determines the relevant transition from the E_{22} band containing j excitons to the relevant E_{11} band. The rate constants for the linear relaxation ($K^{(i)}$) and nonlinear annihilation ($\Gamma^{(i)}$) determine the exciton loss from the E_{11} band already containing i excitons. It is also assumed that after annihilation the excitons from the $E_{nn} \cong 2E_{11}$ electronic band can relax either to the E_{22} band (with probability α) or directly back to the E_{11} band with probability $(1 - \alpha)$. According to the scheme shown in Figure 6, the following master equations for the occupation probabilities $P_{i,j}$ are derived:

$$\frac{dP_{0,0}}{dt} = -\{G_1^{(0)}(t) + G_2^{(0)}(t)\}P_{0,0} + K^{(1)}P_{1,0} \quad (6)$$

$$\frac{dP_{1,0}}{dt} = G_1^{(0)}(t)P_{0,0} - \{G_1^{(1)}(t) + G_2^{(0)}(t) + K^{(1)}\}P_{1,0} + k_{21}^{(1)}P_{0,1} + \{K^{(2)} + (1-\alpha)\Gamma^{(2)}\}P_{2,0} \quad (7)$$

$$\frac{dP_{0,1}}{dt} = G_2^{(0)}(t)P_{0,0} - \{G_1^{(0)}(t) + G_2^{(1)}(t) + k_{21}^{(1)}\}P_{0,1} + \alpha\Gamma^{(2)}P_{2,0} + K^{(1)}P_{1,1} \quad (8)$$

etc. For $P_{i,j}$ when $i \geq 2$ and $j \geq 1$, the relevant equations can be given by

$$\frac{dP_{i,0}}{dt} = G_1^{(i-1)}(t)P_{i-1,0} - \{G_1^{(i)}(t) + G_2^{(0)}(t) + K^{(i)} + \Gamma^{(i)}\}P_{i,0} + k_{21}^{(1)}P_{i-1,1} + \{K^{(i+1)} + (1-\alpha)\Gamma^{(i+1)}\}P_{i+1,0} \quad (9)$$

dx.doi.org/10.1021/jp106250a |J. Phys. Chem. B 2011, 115, 5201–5211

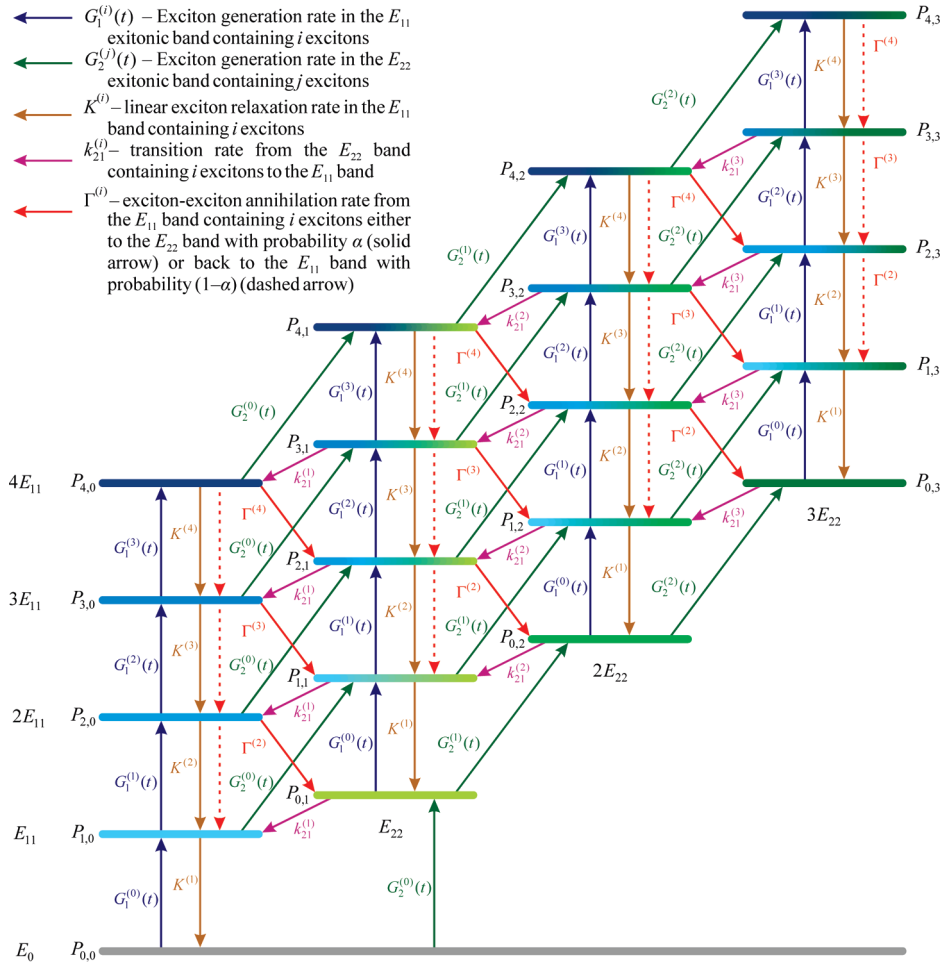

Figure 6. The kinetic scheme for the system with multiple exciton population of both E_{11} and E_{22} exciton states. The lowest energy level E_0 (gray bar) indicates the ground state. The population of the E_{11} exciton band is reflected in the upward direction with the corresponding energies of E_{11}, $2E_{11}$, $3E_{11}$, ... (shown up to $4\,E_{11}$), while the population of the E_{22} exciton band is indicated rightwards (with the corresponding energies of E_{22}, $2E_{22}$, ... (shown up to $3E_{22}$)). In addition, the levels of the combined population corresponding to energies $E_{i,j} = i \cdot E_{11} + j \cdot E_{22}$ are also shown. The probabilities of the occupation of these energy levels are denoted as $P_{i,j}$, and the possible transition pathways between different states are indicated with arrows (for the labeling, see the legend in the kinetic scheme). For clarity, the upper electronic band $E_{nn} \cong 2E_{11}$ involved in exciton−exciton annihilation is not shown, since the excitons relax from this state almost instantaneously (comparing with other characteristic rates in this model) either to the E_{22} or back to the E_{11} band.

$$\frac{dP_{0,j}}{dt} = G_2^{(j-1)}(t)P_{0,j-1} - \{G_1^{(0)}(t) + G_2^{(j)}(t) + k_{21}^{(j)}\}P_{0,1} + \alpha\Gamma^{(2)}P_{2,j-1} + K^{(1)}P_{1,j} \quad (10)$$

$$\frac{dP_{1,j}}{dt} = G_2^{(j-1)}(t)P_{1,j-1} + G_1^{(0)}(t)P_{0,j} - \{G_1^{(1)}(t) + G_2^{(j)}(t) + K^{(1)} + k_{21}^{(j)}\}P_{1,j} + k_{21}^{(j+1)}P_{0,j+1} + \alpha\Gamma^{(3)}P_{3,j-1} + \{K^{(2)} + (1-\alpha)\Gamma^{(2)}\}P_{2,j} \quad (11)$$

$$\frac{dP_{i,j}}{dt} = G_2^{(j-1)}(t)P_{i,j-1} + G_1^{(i-1)}(t)P_{i-1,j} - \{G_1^{(i)}(t) + G_2^{(j)}(t) + K^{(i)} + k_{21}^{(j)} + \Gamma^{(i)}\}P_{i,j} + k_{21}^{(j+1)}P_{i-1,j+1} + \alpha\Gamma^{(i+2)}P_{i+2,j-1} + \{K^{(i+1)} + (1-\alpha)\Gamma^{(i+1)}\}P_{i+1,j} \quad (12)$$

Since the annihilation process corresponds to the two-exciton relaxation, the following relationship for the annihilation rates can be deduced if the statistical number of possible relaxation pathways is taken into account:

$$\Gamma^{(i)} = \frac{i(i-1)}{2}\Gamma^{(2)} \equiv i(i-1)\frac{\gamma}{2} \quad (13)$$

Similarly, for the linear relaxation rates, we obtain

$$k_{21}^{(i)} = ik_{21}^{(1)} \equiv ik_{21} \quad (14)$$

and

$$K^{(i)} = iK^{(1)} \equiv iK \quad (15)$$

Substituting eqs 13−15 into eqs 6−12 and also assuming that the exciton generation rate is independent of i and j, i.e., $G_1^{(i)}(t) \equiv G_1(t)$ and $G_2^{(j)}(t) \equiv G_2(t)$, we get

$$\frac{dP_{0,0}}{dt} = -\{G_1(t) + G_2(t)\}P_{0,0} + KP_{1,0} \quad (16)$$

$$\frac{dP_{1,0}}{dt} = G_1(t)P_{0,0} - \{G_1(t) + G_2(t) + K\}P_{1,0} + k_{21}P_{0,1} + \{2K + (1-\alpha)\cdot\gamma\}P_{2,0} \quad (17)$$

dx.doi.org/10.1021/jp106250a |J. Phys. Chem. B 2011, 115, 5201–5211

$$\frac{dP_{i,0}}{dt} = G_1(t)P_{i-1,0} - \left\{G_1(t) + G_2(t) + iK + i(i-1)\frac{\gamma}{2}\right\}P_{i,0} + k_{21}P_{i-1,1} + \left\{(i+1)K + (1-\alpha)(i+1)i\frac{\gamma}{2}\right\}P_{i+1,0} \quad (18)$$

$$\frac{dP_{0,j}}{dt} = G_2(t)P_{0,j-1} - \{G_1(t) + G_2(t) + jk_{21}\}P_{0,j} + \alpha\cdot\gamma P_{2,j-1} + KP_{1,j} \quad (19)$$

$$\frac{dP_{1,j}}{dt} = G_2(t)P_{1,j-1} + G_1(t)P_{0,j} - \{G_1(t) + G_2(t) + K + jk_{21}\}P_{1,j} + (j+1)k_{21}P_{0,j+1} + \alpha\cdot 3\cdot\gamma P_{3,j-1} + \{2K + (1-\alpha)\cdot\gamma\}P_{2,j} \quad (20)$$

$$\frac{dP_{i,j}}{dt} = G_2(t)P_{i,j-1} + G_1(t)P_{i-1,j} - \left\{G_1(t) + G_2(t) + iK + jk_{21} + i(i-1)\frac{\gamma}{2}\right\}P_{i,j} + (j+1)k_{21}P_{i-1,j+1} + \alpha(i+2)(i+1)\frac{\gamma}{2}P_{i+2,j-1} + \left\{(i+1)K + (1-\alpha)(i+1)i\frac{\gamma}{2}\right\}P_{i+1,j} \quad (21)$$

for $i \geq 2$ and $j \geq 1$.

The amount of excitons in the E_{11} and E_{22} bands can also be defined accordingly as

$$n_1(t) = \sum_{i,j} i\cdot P_{i,j}(t), \qquad n_2(t) = \sum_{i,j} j\cdot P_{i,j}(t) \quad (22)$$

Thus, to determine the temporal evolution of the excitations in the system, the set of differential equations (eqs 16−21) has to be solved. The amount of these equations increases with the excitation intensity but is restricted when the population reaches the limits as a result of phase space filling. If the amount of exciton states in the phase space (N_1 for the E_{11} manifold and N_2 for the E_{22} manifold) is taken into account, the set of equations to be solved reaches a finite number, which is equal to $(N_1 + 1) \times (N_2 + 1)$. As a result, the exciton kinetics should become intensity-independent for excitation intensities large enough to approach the limit of the phase space filling.

According to the experimental conditions, we assume a Gaussian pump pulse with an amplitude A and a fwhm duration of 50 fs. The maximum amounts of exciton states in the phase space for the E_{11} and E_{22} manifolds are assumed to be $N_1 = N_2 = 50$, and the amplitude A of the excitation pulse is chosen to ensure the occurrence of the phase space saturation effect. In our case, the excitation kinetics become almost independent of A when it is greater than ~1.2 (when neglecting phase space filling factors and when the exciton relaxation/annihilation processes are switched off, this would result in generation of about 60 excitons per nanotube). Thus, we assume A = 1.7 in all our subsequent simulations. The linear relaxation rate from the E_{11} manifold is assumed to be equal to K^{-1} = 10 ps. We find that both kinetics measured at room temperature with either E_{11} or E_{22} excitation can be well described for their initial part by assuming the following set of parameters: α = 0.5, γ^{-1} = 460 fs, and k_{21}^{-1} = 400 fs (Figure 7a). On the other hand, for the data collected at 110 K, the best fits are obtained when α = 0.5, γ^{-1} = 770 fs, and k_{21}^{-1} = 390 fs are chosen (Figure 8b). With these parameters, we are also able to obtain the intensity dependences for the maximum value of the bleaching signal, as defined by eq 4, close to the experimental observations. These intensity dependences appear almost the same for the two temperatures (110 and 292 K), as shown in Figure 7c.

It is noteworthy that, similar to the continuous model, an increase of the A value at least up to A = 3 leads to an almost linear increase of the fitting value of γ^{-1}, while, opposite to the continuous model, the calculated kinetics are less sensitive to the changes of the α parameter, the branching ratio. In this case, the sensitivity of the kinetics to the excitation intensity is controlled by an appropriate phase space filling factor.

Within the same annihilation scheme, the much larger differences in the kinetics measured with E_{11} and E_{22} excitation for the DWNTs (see Figure 4) could be attributed to much slower rates of the annihilation γ and the relaxation k_{21}, which may result from the presence of the outer nanotube. Indeed, the best fit of the kinetics for the DWNT is obtained assuming α = 0.5, γ^{-1} = 3930 fs, and k_{21}^{-1} = 800 fs (Figure 8a). Using these parameters, the intensity dependence of the resulting maximal bleaching signal also exhibits a trend similar to the experimental results (Figure 8b). It is evident that our chosen value A = 1.7 corresponds to a situation when both intensity dependences exhibit some saturation effect. As a result, by increasing the A value above ~1.5, the obtained value of γ^{-1} remains almost invariant.

V. DISCUSSION

Through the numerical simulations presented above, we found that the strikingly different dependence of the maximal bleaching signal on the excitation intensity observed for E_{11} and E_{22} excitation (square root dependence vs linear dependence, as shown in Figures 2 and 4b) could be understood in terms of nonlinear annihilation of coherent excitons. In order to reproduce these intensity dependences, we proposed two relaxation pathways from the doubly excited states that are populated in the course of nonlinear exciton−exciton annihilation. One of them takes into account a sequential relaxation from these high-lying excited states via the E_{22} band to the lowest E_{11} band, while the other pathway corresponds to a direct exciton relaxation to the E_{11} band that bypasses the E_{22} band. The branching ratio α between these two pathways, the values of the linear relaxation rate k_{21}, and the values of the nonlinear annihilation rate γ are all sensitive to the phase space filling factors. Through fitting the same experimental data based on the continuum model (Figure 5b) and the stochastic model (Figure 7a), we found that all of these values are markedly different.

It is noteworthy that the phase space filling factors used in the two theoretical models are very different: N_1 and N_2 were chosen to be 2000 for the continuum model and 50 for the stochastic model. Since the initial kinetics have to be independent of the model used for calculations (either the continuum or stochastic model), use of different phase space filling factors and excitation intensities result in differences in α, k_{21}, and γ values needed for the best fits of the experimental data. Moreover, the annihilation rates determined according to the continuum model are also dependent on the excitation intensity, and the defined value of $1/\gamma$ varies linearly with A. However, this is not the case for the stochastic model, where the annihilation rate is found to be

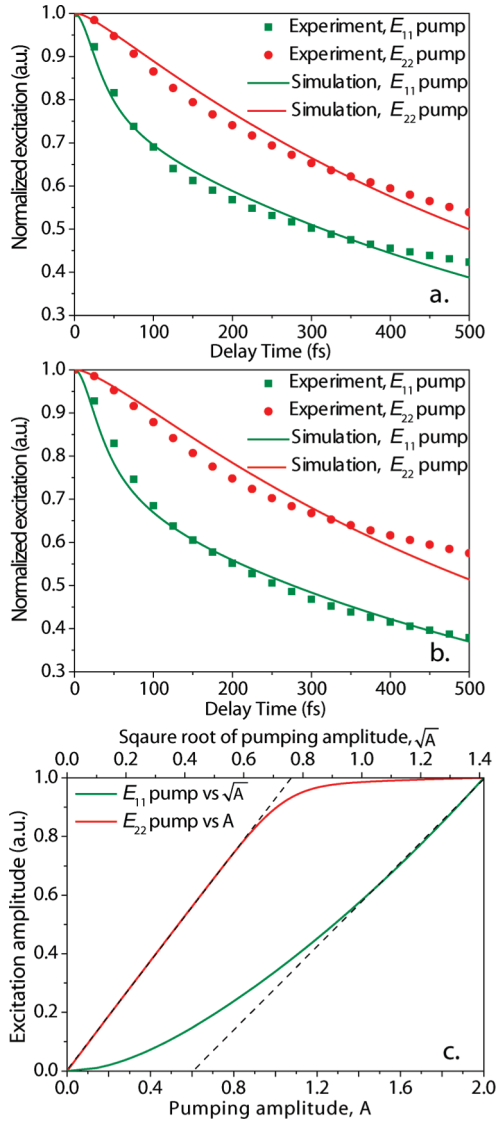

Figure 7. (a) The best fits to the experimental data measured at 292 K (squares and circles) for the (6, 5) tube species calculated according to the stochastic model (solid curves) using the following parametres: $\alpha = 0.5$, $\gamma^{-1} = 460$ fs, $k_{21}^{-1} = 400$ fs. (b) The best fits to the data measured at 110 K for the same tube species obtained using $\alpha = 0.5$, $\gamma^{-1} = 770$ fs, and $k_{21}^{-1} = 390$ fs. (c) The dependence of $(n_1 + n_2)_{max}$ on excitation intensity defined as A in the case of pumping to the E_{22} band (red curve) and on its square root $\sqrt{A}$ in the case of pumping to the E_{11} band (green curve) calculated using the same parameter set. These intensity dependencies exhibit almost the same behavior at both temperatures.

almost independent of the excitation intensity. Indeed, for the chosen phase space filling factors, $N_1 = N_2 = 50$, the saturation of the maximal bleaching signal occurs at very similar excitation intensities for the (7, 5) inner tube of a DWNT species upon pumping its E_{11} or E_{22} state (see Figure 8b). When the excitation intensity exceeds this limiting value, the calculated kinetics remain almost invariant, and the obtained rate parameters (γ and k_{21}) are no longer dependent on the intensity. On the other hand, our calculations for the (6, 5) SWNT species with the same assumption for the phase space filling factors ($N_1 = N_2 = 50$) show that the maximal bleaching signal starts to saturate at a much lower excitation intensity in the case of the E_{22} excitation than the corresponding intensity for the E_{11} excitation

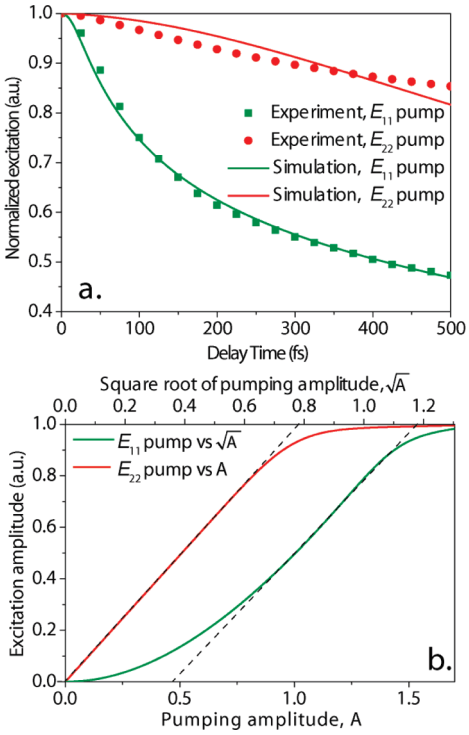

Figure 8. (a) The best fits to the experimental data (squares and circles) collected for the (7, 5) inner tube of the dominant DWNT species calculated according to the stochastic model (solid curves) using the following parameters: $\alpha = 0.5$, $\gamma^{-1} = 3930$ fs, $k_{21}^{-1} = 800$ fs. (b) The dependence of the $(n_1 + n_2)_{max}$ on excitation intensity defined as A in the case of pumping to the E_{22} band (red curve) and on its square root $\sqrt{A}$ in the case of pumping to the E_{11} band (green curve) calculated using the same parameter set.

(Figure 7c). As a result, the calculated kinetics still depend on the excitation amplitude for the chosen intensity in our simulations (A = 1.7), although to a lesser extent than that seen at lower intensities. For much higher excitation intensities where the maximal bleaching signal calculated for the E_{11} excitation starts to saturate, the rate parameters become intensity independent. However, the maximum bleaching signal calculated for the E_{22} excitation would remain invariant within a very wide region for $A > 1.5$. This difference in the intensity dependence for the E_{11} and E_{22} excitation could be overcome by assuming different phase space filling factors for the two excitonic bands ($N_1 < N_2$).

The kinetics measured experimentally can be reasonably well fitted using either the continuum or stochastic models. However, our calculations using the same sets of parameters lead to distinct differences in the dependence of the bleaching signal amplitude on the excitation intensity. The phase space filling factors $f_i(n_i)$ introduced in the equations of the continuum model (eqs 1 and 5) can partly account for the saturation effect found experimentally, and thus such modifications allow us to obtain a similar saturation effect. By taking the phase space filling restriction into account, we obtain from eq 5 (instead of eqs 2 and 3) that

$$n_1(0) \approx \frac{G_{1,\max}}{(1+\alpha)\gamma N_1}\left(\sqrt{1+\frac{2N_1{}^2(1+\alpha)\gamma}{G_{1,\max}}}-1\right), \quad (23)$$

$$n_2(0) \approx 0$$

dx.doi.org/10.1021/jp106250a |J. Phys. Chem. B 2011, 115, 5201–5211

when the pump pulse is in resonance with the E_{11} exciton state, whereas

$$n_1(0) \approx 0, \qquad n_2(0) \approx \frac{G_{2,\max}}{k_{21} + \frac{G_{2,\max}}{N_2}} \tag{24}$$

when the E_{22} exciton state is excited. From eqs 23 and 24, it is clear that the saturation of the bleaching signal amplitude with increasing the excitation intensity is very gradual (see Figure 5a,d), and the discrepancies from eqs 2 and 3 are obvious even at the intermediate intensities of excitation. On the other hand, in the stochastic model, the phase space filling appears naturally when the number of excitons reaches the maximum number of the energy states that are available in the system. This provides a much more abrupt saturation (Figure 7c), which does not manifest itself at intermediate values of the excitation intensity, and thus is in better agreement with experimental observations.

With the same stochastic model, we are able to reproduce quantitatively the initial portion of the kinetics and qualitatively the intensity dependence of the maximum bleaching signals by assuming only slower rates k_{21} and γ (Figures 7 and 8). The nonlinear annihilation kinetics calculated in the frame of the stochastic model exhibit slower decay for delay times >400 fs than the corresponding kinetics obtained according to the continuum model.[15,16,31] However, this slow-down is still insufficient to describe the kinetics observed experimentally. This is in contrast to the data obtained from our previous studies on aqueous solutions of semiconducting SWNTs, where nonlinear annihilation of coherent excitons was identified as the leading relaxation process at room temperature.[10,13,14] This discrepancy between our present and previous results suggests a possible sample dependence of exciton relaxation dynamics. In view of the strong environmental effects on exciton dynamics observed by both single-tube and ensemble time-resolved experiments,[8,32] it may not be surprising that the variation of nanotube surroundings can affect the mechanisms of exciton−exciton annihilation.

As follows from qualitative analysis of the experimental data, a plot of the transient absorption kinetics measured at room temperature by $(\Delta OD_0/\Delta OD(t) - 1)^2$ scales linearly with time for long delay times (picoseconds and longer), and thus can be attributed to the 1D diffusion-limited annihilation.[29] It indicates a change of the physical mechanism of exciton−exciton annihilation from involving delocalized coherent excitons to localized excitons on the intermediate time scale, from a few hundreds of fs up to 1 ps (see Figures 3c and 4b). This possible change of physical mechanisms of exciton−exciton annihilation can be understood in the following way. Initially, the exciton density is high enough so that the wave functions of coherent excitons are overlapping in the nanotube. As a result, the nonlinear annihilation process involving coherent excitons dominates. The resulting exciton relaxation leads to a decrease of the concentration of excitons, and consequently their wave functions will no longer overlap. In this case, exciton diffusion becomes a dominant factor in the nonlinear exciton annihilation.[29] Evidently, this mechanistic change in the nonlinear annihilation process will result in a corresponding rate decrease owing to the finite exciton diffusion time scale. Therefore, the kinetics on the intermediate and long times should be attributed to nonlinear annihilation between excitons which are affected by their scattering on the lattice imperfections caused by the external conditions. These external conditions could also stimulate the spontaneous symmetry breaking or so-called Peierls distortion expected in 1-D systems.[33] As a result of these processes, the diffusion-limited annihilation starts to dominate. On the other hand, the data collected at temperatures below 200 K, such as at 110 K (Figure 3d), indicates an annihilation process involving substantially delocalized excitons. This observation is qualitatively in line with the longer exciton dephasing times found at low temperatures.[22]

VI. CONCLUDING REMARKS

A picture is emerging of excitons in semiconducting SWNTs in which the character of the excitation and its dynamical behavior vary remarkably as a function of time following excitation. Using femtosecond transient absorption measurements on the (6, 5) SWNT type and the (7, 5) inner tubes of a dominant DWNT species, we found that the dynamics of exciton relaxation depends strongly on their method of preparation, either directly into E_{11} or via ultrafast relaxation from E_{22}. For excitons created directly in E_{11}, the initial state comprises multiple overlapping coherent excitons. As exciton−exciton interaction does not require exciton motion, rapid exciton−exciton scattering and exciton−exciton annihilation transpires during the initial decay. Following this initial annihilation phase, the remaining excitons may still be coherent for time scales of ~1 ps.[28] Qualitative analysis of the E_{11} transient decay kinetics at longer delay times (>1 ps) supports the occurrence of diffusion-limited exciton−exciton annihilation or quenching kinetics by traps, in agreement with earlier studies of annihilation focused predominately on long time scales.[17,18]

The exciton annihilation process produces complex behavior in the optical response that is sensitive to how the E_{11} state is populated. When E_{22} is initially populated, the subsequent phonon-mediated relaxation leads to exciton occupation at the E_{11} state with various momenta. Relaxation of all these excitons is "visible" in transient absorption experiments: those with close to zero momenta through stimulated emission of the E_{11} state and its excited-state absorption, and the remaining with finite momenta can be observed through ground state recovery. In contrast, direct excitation of the E_{11} state will create excitons with negligible momentum and subsequent relaxation is expected to be more rapid, provided that this process is faster than the thermalization. Experimentally, a clearly slower decay is indeed observed when the E_{22} state of the (6, 5) tubes is excited than the one measured with its E_{11} excitation. This difference is even more pronounced for the (7, 5) inner tube species. Striking differences in the excitation intensity dependence are further found for the maximal bleaching signals obtained for both the (6, 5) and (7, 5) tubes upon excitation of their corresponding E_{22} or E_{11} states. The former exhibits a linear dependence on the E_{22} excitation intensity, whereas the latter scales linearly with the square root of the E_{11} excitation intensity.

In order to better understand these experimental findings, we developed a continuum model and a stochastic model by explicit consideration of the annihilation of coherent excitons and a branching parameter α. Our numerical simulations show that both models can reproduce reasonably well the initial portion of decay kinetics measured upon the E_{22} and E_{11} excitation of the chosen tube species but with significantly different sets of adjustable parameters. In particular, our calculations based on the stochastic model give qualitatively better agreement with the intensity dependence observed experimentally than those obtained with the continuum model. However, it should be pointed out that the differences in momentum distribution depending on how the E_{11} state is populated is not yet fully included in our theoretical model. While the E_{22} to E_{11} transition is present in

our scheme, population distribution in the K_{CM} space of the E_{11} excitons arising from this relaxation is not taken into account. Nevertheless, we believe the kinetic models developed here can provide important insight into how multiple exciton states are involved in the annihilation and impact ionization processes in SWNTs, which may play a key role in practical applications such as development of highly efficient SWNT photodiode devices.[34]

AUTHOR INFORMATION

Corresponding Author

* E-mail: Leonas.Valkunas@ff.vu.lt.

ACKNOWLEDGMENT

This research was supported by the global grant of the Lithuanian Scientific Council according to the operational programme for the human resources development and by the NSF. Y.-Z.M. also acknowledges the support by the Laboratory Directed Research and Development Program of Oak Ridge National Laboratory, managed by UT-Battelle, LLC, for the U.S. Department of Energy. M.W.G. thanks Natural Sciences and Engineering Research Council of Canada for a postgraduate scholarship. Density gradient processing was supported by the National Science Foundation, the Office of Naval Research, and the Nanoelectronics Research Initiative.

REFERENCES

(1) Kittel, C. *Quantum Theory of Solids*; John Willey and Sons: New York, London, 1963.
(2) Wang, F.; Dukovic, G.; Brus, L. E.; Heinz, T. F. *Science* **2005**, *308*, 838.
(3) Ma, Y.-Z.; Valkunas, L.; Bachilo, S. M.; Fleming, G. R. *J. Phys. Chem. B* **2005**, *109*, 15671.
(4) Spataru, C. D.; Ismail-Beigi, S.; Benedict, L. X.; Louie, S. G. *Appl. Phys. A: Mater. Sci. Process.* **2004**, *78*, 1129.
(5) Spataru, C. D.; Ismail-Beigi, S.; Benedict, L. X.; Louie, S. G. *Phys. Rev. Lett.* **2004**, *92*, No. 077402.
(6) He, X.-F. *Phys. Rev. B* **1991**, *43*, 2063.
(7) Korovyanko, O. J.; Sheng, C.-X.; Vardeny, Z. V.; Dalton, A. B.; Baughman, R. H. *Phys. Rev. Lett.* **2004**, *92*, No. 017403.
(8) Ostojic, G. N.; Zaric, S.; Kono, J.; Strano, M. S.; Moore, V. C.; Hauge, R. H.; Smalley, R. E. *Phys. Rev. Lett.* **2004**, *92*, 117402.
(9) Huang, L.; Pedrosa, H. N.; Krauss, T. D. *Phys. Rev. Lett.* **2004**, *93*, No. 017403.
(10) Ma, Y.-Z.; Valkunas, L.; Dexheimer, S. L.; Bachilo, S. M.; Fleming, G. R. *Phys. Rev. Lett.* **2005**, *94*, 157402.
(11) Ma, Y.-Z.; Stenger, J.; Zimmermann, J.; Bachilo, S. M.; Smalley, R. E.; Weisman, R. B.; Fleming, G. R. *J. Chem. Phys.* **2004**, *120*, 3368.
(12) Wang, F.; Dukovic, G.; Knoesel, E.; Brus, L. E.; Heinz, T. F. *Phys. Rev. B* **2004**, *70*, 241403.
(13) Valkunas, L.; Ma, Y.-Z.; Fleming, G. R. *Phys. Rev. B* **2006**, *73*, 115432.
(14) Huang, L.; Krauss, T. D. *Phys. Rev. Lett.* **2006**, *96*, No. 057407.
(15) Barzykin, A. V.; Tachiya, M. *Phys. Rev. B* **2005**, *72*, No. 075425.
(16) Barzykin, A. V.; Tachiya, M. *J. Phys.: Condens. Matter* **2007**, *19*, No. 065105.
(17) Russo, R. M.; Mele, E. J.; Kane, C. L.; Rubtsov, I. V.; Therien, M. J.; Luzzi, D. E. *Phys. Rev. B* **2006**, *74*, No. 041405(R).
(18) Zhu, Z.; Crochet, J.; Arnold, M. S.; Hersam, M. C.; Ulbricht, H.; Resasco, D.; Hertel, T. *J. Phys. Chem. C* **2007**, *111*, 3831.
(19) Srivastava, A.; Kono, J. *Phys. Rev. B* **2009**, *79*, 205407.
(20) Murakami, Y.; Kono, J. *Phys. Rev. Lett.* **2009**, *102*, No. 037401.
(21) Lüer, L.; Hoseinkhani, S.; Polli, D.; Crochet, J.; Hertel, T.; Lanzani, G. *Nat. Phys.* **2009**, *5*, 54.
(22) Ma, Y.-Z.; Graham, M. W.; Fleming, G. R.; Green, A. A.; Hersam, M. C. *Phys. Rev. Lett.* **2008**, *101*, 217402.
(23) Abramavicius, D.; Ma, Y.-Z.; Graham, M. W.; Valkunas, L.; Fleming, G. R. *Phys. Rev. B* **2009**, *79*, 195445.
(24) Arnold, M. S.; Green, A. A.; Hulvat, J. F.; Stupp, S. I.; Hersam, M. C. *Nat. Nanotechnol.* **2006**, *1*, 60.
(25) Kishi, N.; Kikuchi, S.; Ramesh, P.; Sugai, T.; Watanabe, Y.; Shinohara, H. *J. Phys. Chem. B* **2006**, *110*, 24816.
(26) Ma, Y.-Z.; Valkunas, L.; Dexheimer, S. L.; Fleming, G. R. *Mol. Phys.* **2006**, *104*, 1179.
(27) Ma, Y.-Z.; Hertel, T.; Vardeny, Z. V.; Fleming, G. R.; Valkunas, L. Ultrafast spectroscopy of carbon nanotubes. In *Topics Appl. Phys.*; Jorio, A., Dresselhaus, G., Dresselhaus, M. S., Eds.; Springer-Verlag Berlin: Heidelberg, Germany, 2008; Vol. 111, p 321.
(28) Graham, M. W.; Ma, Y.-Z.; Green, A. A.; Hersam, M. C.; Fleming, G. R. "Proc. of SPIE 7600" , 2010.
(29) Valkunas, L.; Trinkunas, G.; Liuolia, V. Exciton annihilation in molecular aggregates. In *Resonance energy transfer*; Andrews, D. L., Demidov, A. A., Eds.; Wiley and Sons: Chichester, U.K., 1999; p 244.
(30) Manzoni, C.; Gambetta, A.; Menna, E.; Meneghetti, M.; Lanzani, G.; Cerullo, G. *Phys. Rev. Lett.* **2005**, *94*, 207401.
(31) Barzda, V.; Gulbinas, V.; Kananavicius, R.; Cervinskas, V.; van Amerongen, H.; van Grondelle, R.; Valkunas, L. *Biophys. J.* **2001**, *80*, 2409.
(32) Hertel, T.; Hagen, A.; Talalaev, V.; Arnold, K.; Hennrich, F.; Kappes, M.; Rosenthal, S.; McBride, J.; Ulbricht, H.; Flahaut, E. *Nano Lett.* **2005**, *5*, 511.
(33) Tretiak, S.; Kilina, S.; Piryatinski, A.; Saxena, A.; Martin, R. L.; Bishop, A. R. *Nano Lett.* **2007**, *7*, 86.
(34) Gabor, N. M.; Zhong, Z.; Bosnick, K.; Park, J.; McEuen, P. L. *Science* **2009**, 1367.